

Boosting Stable and Fast Potassium Storage of Iron Sulfide through Rational Yolk-Shell Design and Ni Doping

Yanmei Gan^{1,2,3}, Jiajie Zhu⁴, Qixin Zhang^{2,3}, Chaoying Wang², Lunhui Guan³ and Yi Zhao^{2*}

¹College of Chemistry, Fuzhou University, Fuzhou 350108, China

²The Straits Institute of Flexible Electronics (SIFE, Future Technologies), Fujian Normal University, Fuzhou 350117, China

³CAS Key Laboratory of Design and Assembly of Functional Nanostructures, Fujian Key Laboratory of Nanomaterials, Fujian Institute of Research on the Structure of Matter, Chinese Academy of Sciences, Fuzhou 350108, China

⁴School of Physics Science and Engineering, Tongji University, Shanghai 200092, China

Corresponding author. E-mail: ifeyzhao@fjnu.edu.cn

n EXPERIMENTAL SECTION

Synthesis of Ni-Fe₃O₄ NPs. Ni-doped Fe₃O₄ NPs were prepared by a typical solvothermal method. 1.7 mmol FeCl₃·6H₂O and 0.3 mmol NiCl₂·6H₂O were dissolved in 5 mL ethylene glycol and 15 mL diethylene glycol with magnetic stirring for 30 min. After addition of 2 g PVP (MW:40000), the mixture was heated to 120 °C and maintained for 1 h. Then, 1.5 g anhydrous sodium acetate was added, and the heating was stopped. After further stirring for 30 min, the obtained green suspension was transferred into a 50 mL Teflon-lined stainless-steel autoclave and kept at 200 °C for 12 h. The product was washed several times with water and ethanol and dried at 80 °C for 12 h.

Synthesis of Y-S Ni-Fe₃O₄@C Composite. In a typical method, 100 mg cetyltrimethylammonium bromide (CTAB) was dissolved in 50 mL mixed solution of ethanol, water, and ammonia (volume ratio of 71.4:10:3.14). Then, 50 mg Ni-doped Fe₃O₄ was dispersed in the above solution and sonicated to form homogeneous solution, followed with the slow addition of 0.5 mL tetraethyl orthosilicate. After stirring for 6 h, the product was filtered and washed via water and ethanol, then dried for 12 h. Next, 90 mg above product was put into 7 mL water and sonicated for 0.5 h, followed by the addition of 25 μL NH₃·H₂O and 0.25 mL 0.01 M CTAB aqueous solution and mechanical stirring for 0.5 h. After adding 12.5 mg resorcinol and 17.5 μL formaldehyde solution, this mixture was kept stirring for 16 h. The brown sample was obtained by filtration, washed with water and ethanol, and dried at 80 °C for 12 h. Finally, the sample was annealed at 450 °C under Ar atmosphere for 2 h and reacted with 40 mL 2 M NaOH aqueous solution for 24 h, obtaining Y-S Ni-Fe₃O₄@C.

Synthesis of Y-S Ni-FeS₂@C Composite. For sulfuration treatment, 20 mg Y-S Ni-Fe₃O₄@C and 40 mg sulfur were ground evenly and sealed in a quartz tube under vacuum, which was then heated to 155 °C for 6 h and 500 °C for 24 h. The obtained product was taken out of the tube and further annealed at 300 °C for 2 h under Ar to sublimate excess sulfur, to achieve Y-S Ni-FeS₂@C. Pure Fe₃O₄, Y-S Fe₃O₄@C, and Y-S FeS₂@C samples were fabricated under the same procedure by using 2 mmol FeCl₃·6H₂O as the precursor.

Materials characterizations. The structure, morphology, and component of the samples were characterized through X-ray diffraction (Shimadzu, Miniflex600), scanning electron microscopy (SEM, SU-8010), transmission electron microscopy (TEM, Tecnai F20), and X-ray photoelectron spectroscopy (XPS, ESCALAB 250 Xi). The surface area and porosity properties were conducted via nitrogen absorption-desorption measurement (Quanta chrome, Autosorb-iQ2-XR). The weight contents of active materials were calculated based on thermogravimetry analyses (TGA, NETZSCH STA449C).

Computational Method. The total energy calculations were performed based on the density functional theory and the projector augmented plane-wave method, as implemented in the Vienna ab initio simulation package. The Perdew-Burke-Ernzerhof form generalized gradient approximation is taken into account in the exchange-correlation potential. The cut-off energy for plane wave is set to 270 eV. The Kohn-Sham equation is iteratively solved with an energy criterion of 10⁻⁵ eV. The Brillouin zone integration is performed by a 2×2×2 k-mesh for the geometry optimization and a 3×3×3 k-mesh for the electronic structure. A supercell containing 2×2×2 unit cells is used to describe Ni doping at the Fe site in FeS₂. The residual forces on the atoms are less than 0.05 eV/Å after geometry optimization.

Electrochemical Measurements. The battery performance of the composites was conducted via coin-type test cells (CR2025). The working electrode was composed of active materials, ketjen black carbon, and polyvinylidene difluoride in a mass ratio of 7:1.5:1.5 ground evenly with N-methyl pyrrolidone. The obtained slurry was coated on the surface of nickel foam and dried at 80 °C under vacuum for 12 h. Cells were assembled in an Ar-filled glove box. Potassium metal was used as the counter electrode and the separator was a glass fiber membrane (Whatman, GF/D). The electrolyte was 1 M KFSI in ethylene carbonate (EC):propylene carbonate (PC) (1:1 in volume). The mass loading per electrode was around 0.6–1.2 mg/cm², and the amount of electrolyte used was around 200 μL per cell. Cells were discharged and charged on a LAND battery tester at room temperature from 0.05 to 2.8 V. The cyclic voltammetry (CV) test was performed on an electrochemical workstation (CHI660e) at 0.2 mV s⁻¹.

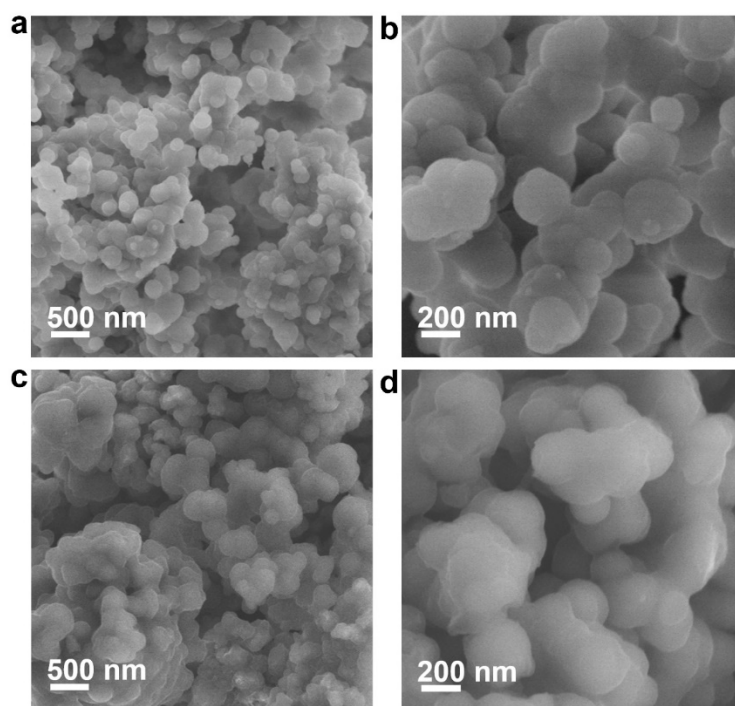


Figure S1. SEM images of (a–b) Ni-Fe₃O₄@SiO₂ and (c–d) Ni-Fe₃O₄@SiO₂@RF.

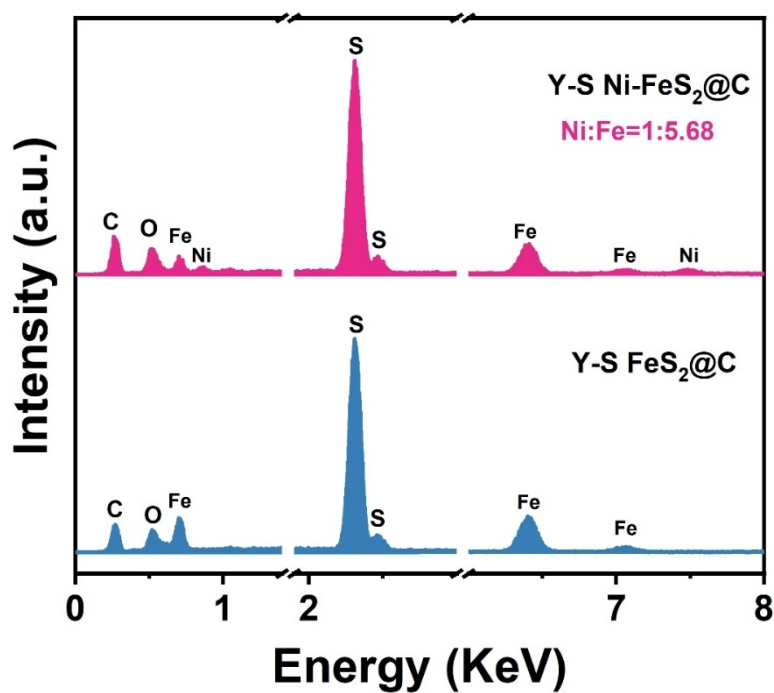


Figure S2. EDS spectrum of Y-S Ni-FeS₂@C and Y-S FeS₂@C composites.

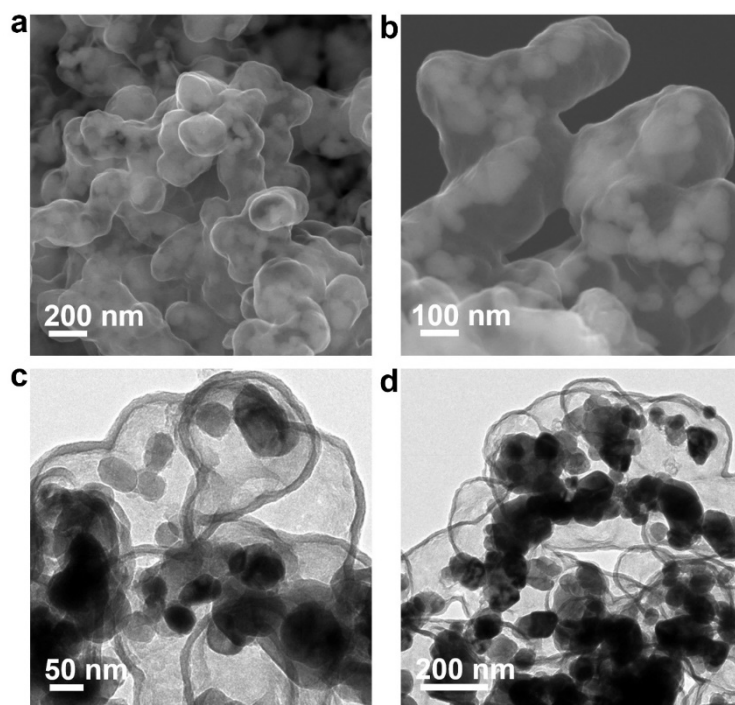


Figure S3. (a–b) SEM, and (c–d) TEM images of Y-S FeS₂@C composite.

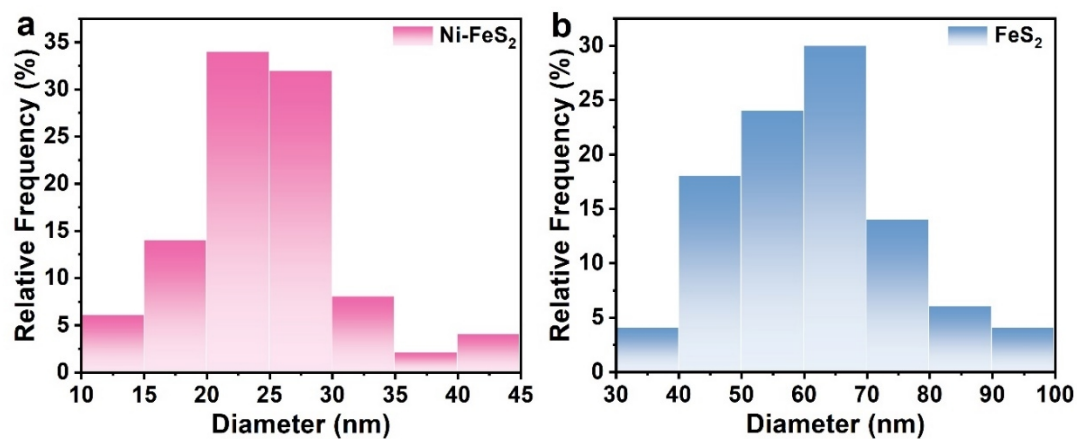


Figure S4. Particle size distribution of (a) Ni-FeS₂ in Y-S Ni-FeS₂@C composite and (b) FeS₂ in Y-S FeS₂@C composites.

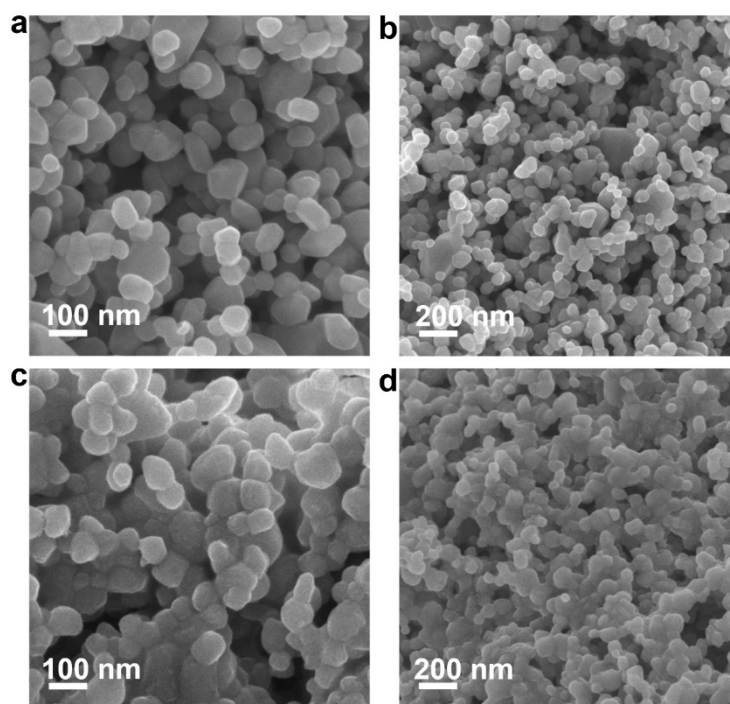


Figure S5. SEM images of (a–b) pure FeS_2 , and (c–d) Ni-FeS_2 nanoparticles.

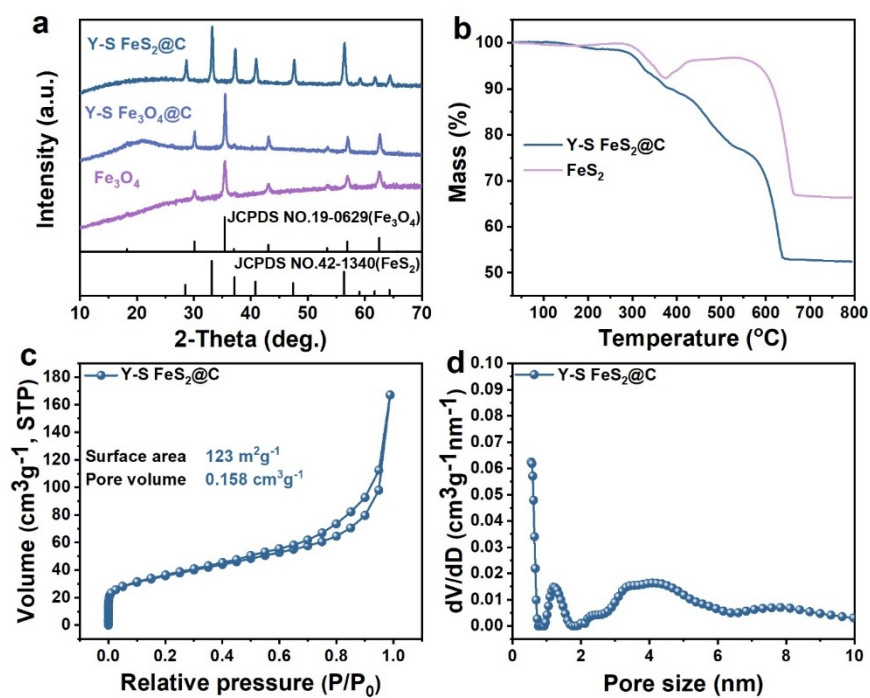


Figure S6. (a) XRD patterns of Fe₃O₄, Y-S Fe₃O₄@C, and Y-S FeS₂@C composites. (b) TGA curves of FeS₂ and Y-S FeS₂@C. (c) N₂ adsorption-desorption isotherm and (d) pore size distribution of Y-S FeS₂@C composite.

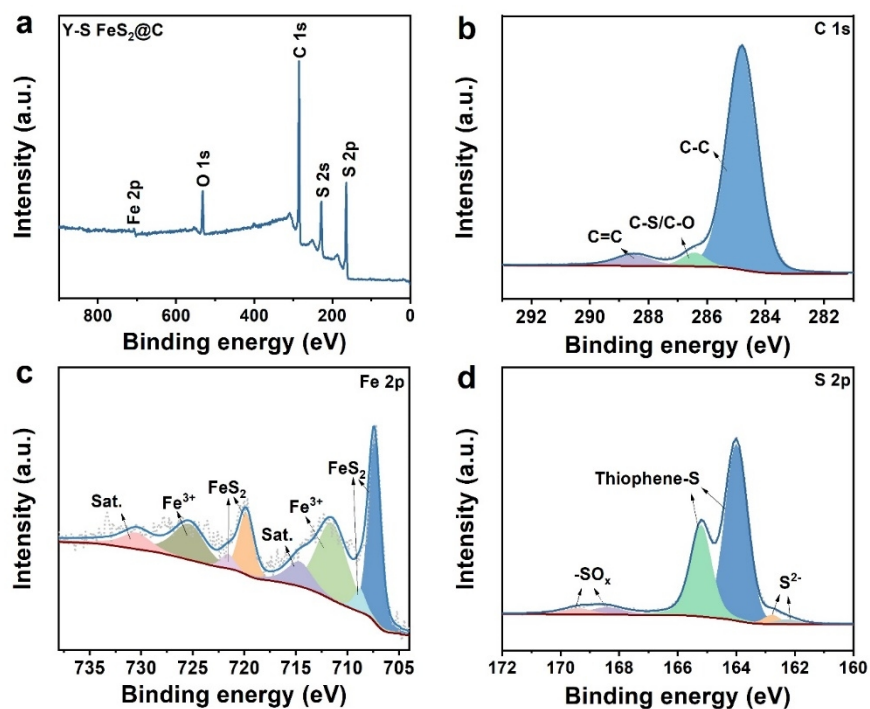


Figure S7. (a) XPS survey profile of Y-S FeS₂@C and the high-resolution spectrum of (b) C 1s, (c) Fe 2p, and (d) S 2p.

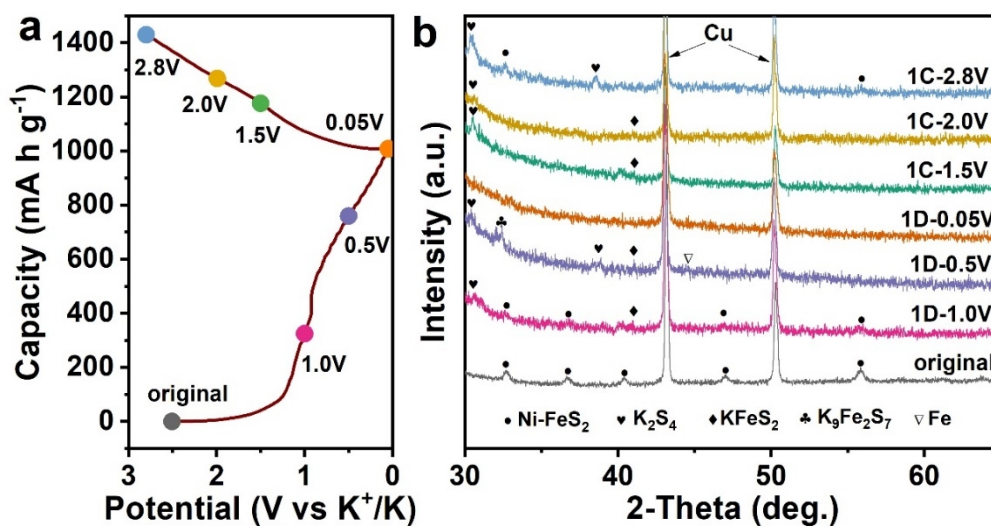


Figure S8. (a) Initial discharge/charge profiles of Y-S Ni-FeS₂@C electrode at 100 mA g⁻¹, and (b) the related ex-situ XRD patterns under various states for PIBs.

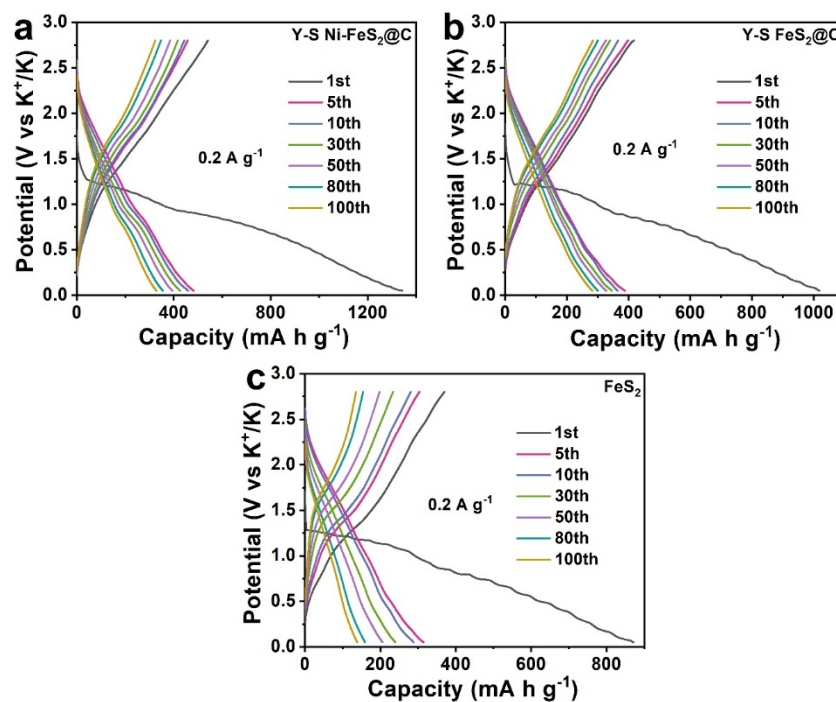


Figure S9. Representative discharge and charge profiles at selected cycles of (a) Y-S Ni-FeS₂@C, (b) Y-S FeS₂@C, and (c) FeS₂ anodes at 0.2 A g⁻¹ for PIBs.

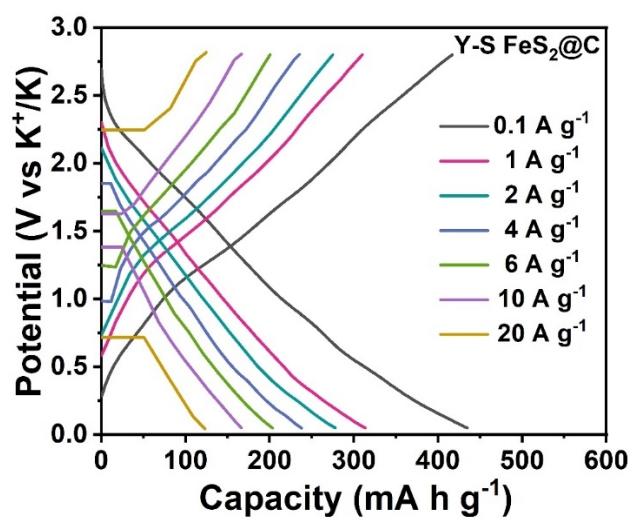


Figure S10. Discharge/charge curves of Y-S FeS₂@C anode at various current densities from 0.01 to 20 A g⁻¹ for PIBs.

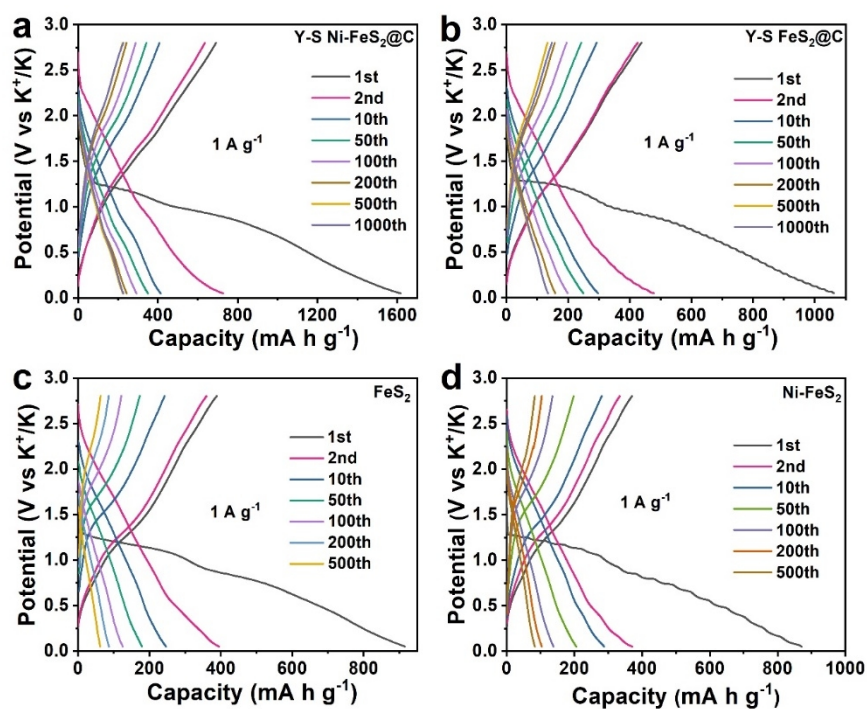


Figure S11. Representative discharge and charge profiles at selected cycles of (a) Y-S Ni-FeS₂@C, (b) Y-S FeS₂@C, (c) FeS₂, and (d) Ni-FeS₂ anodes at 1 A g⁻¹ for PIBs.

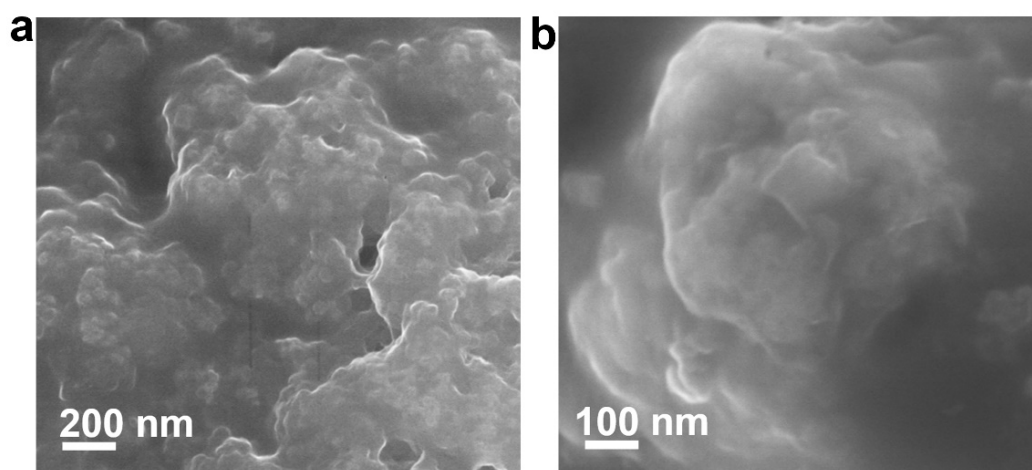


Figure S12. SEM images of Y-S Ni-FeS₂@C electrode after 100 cycles.

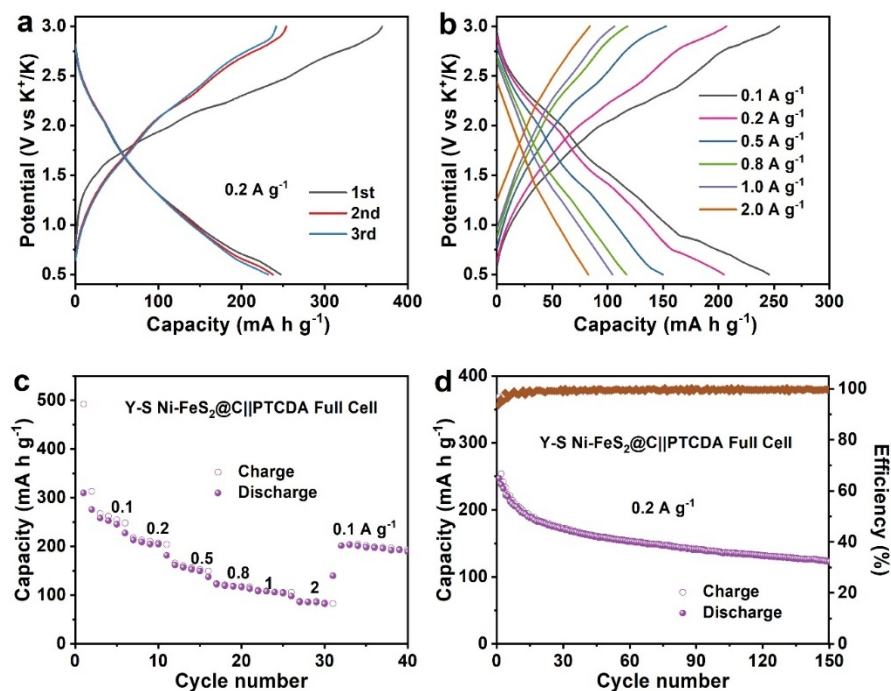


Figure S13. Electrochemical performance of Y-S Ni-FeS₂@C||PTCDA PIB full cell at a voltage range of 0.05 and 3.0 V. (a) Initial three discharge/charge profiles at 0.2 A g⁻¹, (b) typical discharge/charge curves under various rates, (c) rate performance from 0.1 to 2.0 A g⁻¹, and (d) cycling stability at a current density of 0.2 A g⁻¹.

Table S1. Comparison of Y-S Ni-FeS₂@C Composite and As-reported Anodes for PIBs

Anode materials	Current density (A g ⁻¹)	Cycle number	Capacity (mA h g ⁻¹)	Rate capacity (mA h g ⁻¹ /A g ⁻¹)	Ref.
FeS ₂ @HCS	2	100	242	302/2	[1]
FeS ₂ /C@C	0.1	100	262	175/0.5	[2]
Fe _{1-x} S	1	250	212.9	53.1/5	[3]
MoS ₂ @HPCS	1	500	126.2	93.1/2	[4]
Ni-Fe-S-CNTs	0.1	50	181	26/1.6	[5]
Y-S Ni _{0.5} Fe _{0.5} S@C	0.1	250	297	52/5	[6]
FeSe ₂ /N-C	0.2	100	256	155/2	[7]
FeS ₂ @G@CNF	1	680	120	171/1	[8]
SnS@HMCFS	1	1000	245.5	141/5	[9]
Fe ₇ S ₈ @CNT@3DFG	0.05	200	454	160/5	[10]
Y-S FeS₂@C	1	1000	162	166/15	[11]
FeS₂@NC	2	5000	73.6	154.7/10	[12]
FeS₂@C@NS	1	1000	381.7	223.8/8	[13]
FeS₂@C	0.1	300	292	137/5	[14]
FeS₂@rGO	0.5	420	123	151/0.5	[15]
Y-S Ni-FeS₂@C	0.2	100	328.4	232.7/10	This work
	1	1000	223	199.5/20	

n REFERENCES

- (1) Ju, J.; Xu, A.; Song, Y.; Sun, H.; Fu, L.; Yan, Y.; Wu, S. FeS₂ nanoparticles encapsulated in N/S-doped hollow carbon spheres as anode materials for potassium-ion batteries. *ACS Appl. Nano Mater.* **2021**, 4, 4863–4871.
- (2) Li, X.; Wang, H. P.; Zhang, W. C.; Feng, Y. Z.; Ma, J. M. S-doped carbon-coated FeS₂/C@C nanorods for potassium storage. *Acta Metallurgica Sinica (English Letters)* **2020**, 34, 321–328.
- (3) Wu, Y. H.; Xu, R.; Wang, Z. J.; Hao, X. R.; Zhang, C. L.; Zhao, H. P.; Li, W.; Wang, S. Z.; Dong, Y. L.; Huang, Z. T. Carbon-free crystal-like Fe_{1-x}S as an anode for potassium-ion batteries. *ACS Appl. Mater. Interfaces* **2021**, 13, 55218–55226.
- (4) Hu, J. X.; Xie, Y. Y.; Zhou, X. L.; Zhang, Z. A. Engineering hollow porous carbon-sphere-confined MoS₂ with expanded (002) planes for boosting potassium-ion storage. *ACS Appl. Mater. Interfaces* **2020**, 12, 1232–1240.
- (5) Zhang, S. P.; Wang, G.; Wang, B. B.; Wang, J. M.; Bai, J. T.; Wang, H. 3D carbon nanotube network bridged hetero-structured Ni-Fe-S nanocubes toward high-performance lithium, sodium, and potassium storage. *Adv. Funct. Mater.* **2020**, 30, 2001592.
- (6) Yang, S. H.; Park, S. K.; Park, G. D.; Kim, J. H.; Kang, Y. C. Rational synthesis of uniform yolk-shell Ni-Fe bimetallic sulfide nanoflakes@porous carbon nanospheres as advanced anodes for high-performance potassium-/sodium-ion batteries. *Chem. Eng. J.* **2021**, 417, 127963.
- (7) Min, H.; Li, M. H.; Shu, H.; Zhang, X. Q.; Hu, T.; Wang, W. X.; Zhou, Y. J.; Jian, J.; Wang, X. FeSe₂ nanoparticle embedded in 3D honeycomb-like N-doped carbon architectures coupled with electrolytes engineering boost superior potassium ion storage. *Electrochimica Acta* **2021**, 366, 137381.
- (8) Chen, C. M.; Yang, Y. C.; Tang, X.; Qiu, R.; Wang, S.; Cao, G.; Zhang, M. Graphene-encapsulated FeS₂ in carbon fibers as high reversible anodes for Na⁺/K⁺ batteries in a wide temperature range. *Small* **2019**, 15, 1804740.
- (9) He, Y. A.; Xu, Y. F.; Zhang, M.; Xu, J. Z.; Chen, B. B.; Zhang, Y. X.; Bao, J. C.; Zhou, X. S. Confining ultrafine SnS nanoparticles in hollow multichannel carbon nanofibers for boosting potassium storage properties. *Science Bulletin* **2021**, 67, 151–160.
- (10) Han, K.; An, F. Q.; Wan, Q.; Xing, L. D.; Wang, L.; Liu, Q.; Wang, W.; Liu, Y. C.; Li, P.; Qu, X. H. Confining pyrrhotite Fe₇S₈ in carbon nanotubes covalently bonded onto 3D few-layer graphene boosts potassium-ion storage and full-cell applications. *Small* **2021**, 17, 2006719.
- (11) Zhao, Y.; Zhu, J.; Ong, S. J. H.; Yao, Q.; Shi, X.; Hou, K.; Xu, Z. J.; Guan, L. High-rate and ultralong cycle-life potassium ion batteries enabled by in situ engineering of yolk-shell FeS₂@C structure on graphene matrix. *Adv. Energy Mater.* **2018**, 8, 1802565.
- (12) Wu, H.; Lu, S.; Xu, S.; Zhao, J.; Wang, Y.; Huang, C.; Abdelkader, A.; Wang, W. A.; Xi, K.; Guo, Y.; et al. Blowing iron chalcogenides into two-dimensional flaky hybrids with superior cyclability and rate capability for potassium-ion batteries. *ACS Nano* **2021**, 15, 2506–2519.
- (13) Chen, B.; Ding, J.; Bai, X.; Zhang, H.; Liang, M.; Zhu, S.; Shi, C.; Ma, L.; Liu, E.; Zhao, N. et al. Engineering pocket-like graphene-shell encapsulated FeS₂: inhibiting polysulfides shuttle effect in potassium-ion batteries. *Adv. Funct. Mater.* **2021**, 2109899.
- (14) Du, Y.; Weng, W.; Zhang, Z.; He, Y.; Xu, J.; Sun, J.; Liao, J.; Bao, J.; Zhou, X. Candied-haws-like architecture consisting of FeS₂@C core-shell particles for efficient potassium storage. *ACS Mater. Lett.* **2021**, 3, 356–363.
- (15) Xie, J.; Zhu, Y.; Zhuang, N.; Lei, H.; Zhu, W.; Fu, Y.; Javed, M. S.; Li, J.; Mai, W. Rational design of metal organic framework-derived FeS₂ hollow nanocages@reduced graphene oxide for K-ion storage. *Nanoscale* **2018**, 10, 17092–17098.